Supporting Information for ”Direct monitoring of the conformational equilibria of the activation loop in the mitogen-activated protein kinase p38α”

Patrick Roser, Jörn Weisner, Jeffrey R. Simard, Daniel Rauh and Malte Drescher*

Table of Contents

Experimental Procedures

Expression, purification and spin labeling of p38α

N-terminally His_6-tagged p38*α* constructs containing a PreScission Protease cleavage site and the mutations required for mono-labeling (C119S/C162S/F327L/A172C) were generated *via* site-directed mutagenesis and cloned into a pOPINF vector. Human p38*α* MAPK mutant constructs were subsequently transformed into chemically competent BL21 (DE3) *E. coli*, expressed and purified as described previously.[1] Briefly, overexpression was performed at 18 °C overnight (20 hours) while shaking at 160 rpm. Afterwards, the target proteins were purified by Ni-affinity, anion exchange, and size exclusion chromatography. The His_6-tag was removed by addition of PreScission Protease prior to anion exchange chromatography. Finally, purified proteins were concentrated to approximately 20 mg/mL, snap frozen in liquid nitrogen and stored at -80 °C until further use.

Spin labeling of p38α: To a 50 µM solution of p38α in labeling buffer (Tris 20 mM, 200 mM NaCl, 5% v/v glycerol, pH 7.4) three equivalents of (1-oxyl-2,2,5,5-tetramethylpyrroline-3-methyl) methanethiosulfonate, (SCBT, 25 mM in DMSO) were added and incubated overnight at 4 °C while shaking gently. The crude product was isolated using Vivaspin 4 centrifugal filters (10 kDa MWCO, Sartorius) for 6-8 times at 4 °C until no free spin label could be detected using CW EPR spectroscopy. The residue was collected in buffer to yield a final concentration of approx. 300 µM and stored at -80 °C. Labeling efficiency was evaluated using mass spectrometry (Figure S1).

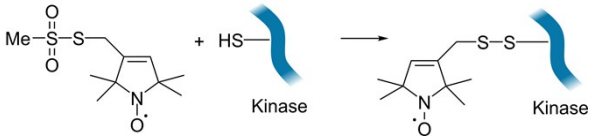

Figure S1. Spin labeling using MTSSL ((1-oxyl-2,2,5,5-tetramethylpyrroline-3-methyl) methanethiosulfonate), which is attached to a cysteine residue.

HTRF-based activity measurements

Prior to activity measurements, p38α kinase constructs (wild-type, mutant/unlabelled, mutant/labelled) were activated with constitutively active $MKK6^{S207E/T211E}$ (Thermo Scientific, Lot# 877061F) in activation buffer (50 mM Tris, 10 mM MgCl2, 1 mM ATP, 1 mM DTT, 0.001 % Tween 20, pH 7.4) at 37 °C for 90 min with shaking at 400 rpm. The reaction mixtures were subsequently dialyzed overnight at 4 °C against storage buffer (20 mM HEPES, 50 mM NaCl, 5 % glycerol, pH 7.1), concentrated to ~0.2 mg/mL and stored at -80 °C for further use.

Activity-based measurements were carried out using the HTRF® KinEASE™ assay from Cisbio according to the manufacturer's instructions. For determination of ATP K_m values, 0.04/3.5/20 ng of activated p38α MAPK constructs (wild-type, mutant/unlabelled, and mutant/labelled, respectively) per well were incubated with varying concentrations of ATP (0.4-900 µM) and 1 µM of GST-ATF2 protein substrate in reaction buffer (50 mM HEPES, 0.1 mM Na3VO4, 0.02 % NaN3, 0.01 % (w/v) BSA, 10 mM MgCl2, 1 mM MnCl2, 1 mM DTT, 0.01 % Triton X-100, pH 7.0) in microtiter plates (Greiner Bio-One, 384 well, black, flat bottom) for 10/10/20 min. Afterwards, the reaction was stopped by addition of detection solution (50 mM HEPES, 0.1 % (w/v) BSA, 800 mM KF, 20 mM EDTA, 0.666 nM anti-phospho-ATF2-Eu(K) antibody, 100 nM anti-GST-d2 antibody, pH 7.0) and incubation for 60 min at room temperature. Finally, fluorescence was detected at emission wavelengths of 620 nm and 665 nm 60 µs after excitation at 317 nm using an EnVision 2104 plate reader (Perkin Elmer). The acceptor/donor ratios ($fl_{665\ nm}/fl_{620\ nm}$) were calculated, plotted versus the ATP concentrations and data were fit to the Michaelis-Menten equation using Origin (OriginLab, Northampton, MA).

Table S1. Determination of ATP Km values for p38α constructs (wild-type, mutant/unlabelled, mutant/labelled) given as mean ± SD (n = 3).

construct	ATP K_m / µM
p38α wild-type	11.0 ± 2.1
p38α mutant/unlabelled	52.3 ± 8.9
p38α mutant/labelled	42.4 ± 7.3

Spin labeling efficiency

After labeling and isolation of the product, the labeling efficiency was evaluated using mass spectrometry. The data showed quantitative single labeling (expected mass 41369 Da) with neglectable signal rising from unlabeled p38α (expected mass 41185 Da) or doubly labeled protein (expected mass 41553 Da).

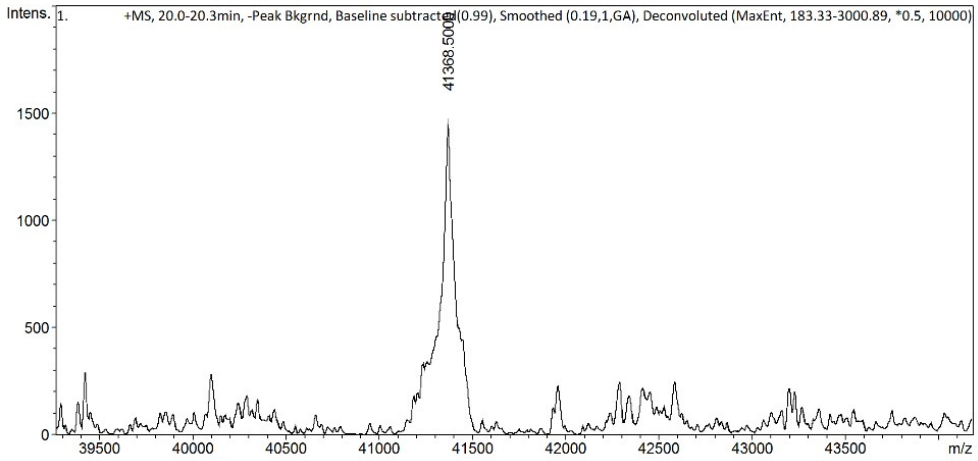

Figure S2. Mass spectrometric analyzation of the labeled p38α showing quantitative single labeling.

Inhibition assay

Inhibition assay: p38α at a concentration of 50-100 µM was mixed with varying amounts of the inhibitors RL45, RL48, Sorafenib, Regorafenib, Skepinone-L, SKF-86002, and SB203580 (10 mM in DMSO stock solutions) to yield a final molar ratio of p38α:inhibitor of 1:3, 1:6 or 1:12. The mixture was incubated for 90 min at 21 °C while gently shaking the flask. The final amount of DMSO in the samples did not exceed 5% in any measurement.

Continuous wave EPR measurements

Spectra were collected at room temperature (293 K) using a Bruker EMX Nano X-Band spectrometer. An aliquot (30 µL) of the protein at concentrations ranging from 50-100 µM was placed in quartz capillaries with an inner diameter of 1 mm. In all cases, the experimental parameters were optimized to yield a high signal-to-noise ratio without distorting the spectral line shape. Quantitative spin counting was carried out using the built-in features of the Bruker Xenon software in addition to the use of spin label stock solutions as a control reference. Spectra normalization was performed by dividing the spectra by the area defined by the double integral.

Temperature dependent measurements were collected using a magnettech MS 5000 X-Band spectrometer equipped with a TC H04 temperature controller. The temperature was varied between 5°C and 32.5°C and spectra were collected using optimized settings as described above.

Post-processing of CW EPR spectra to remove free spin label signal

The experimental spectra contain a small contribution caused by free spin label still present after the isolation procedure. To remove this excess signal from the spectra, a reference spectrum (MTSSL in solution) was adjusted in intensity and subtracted from the data.

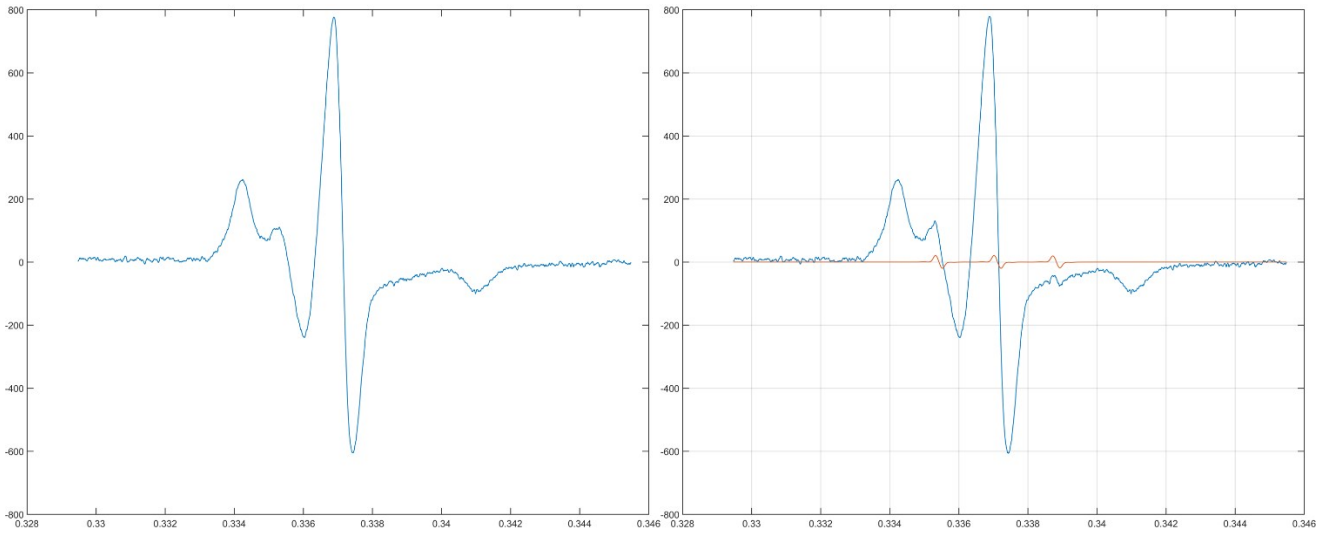

Figure S3. Left: CW EPR spectrum of p38α after labeling (blue). A small amount of free spin label could still be detected in solution. This signal was subtracted from the experimental data using size adjusted spectra obtained from MTSSL in solution (red). Right: Resulting EPR spectrum.

PyMOL simulations

Based on the crystal structure 1A9U of p38α bound to an inhibitor we simulated possible spin label tether rotamers using the PyMOL plugin MTSSL-Wizard (Speed: Thorough, vdW restraints: tight, see Figure S4). [2] This simulation revealed steric hindrance of the spin label attached to the activation loop. This is in agreement with an anisotropic tumbling of the spin label as reflected in the spectral simulations (see below).

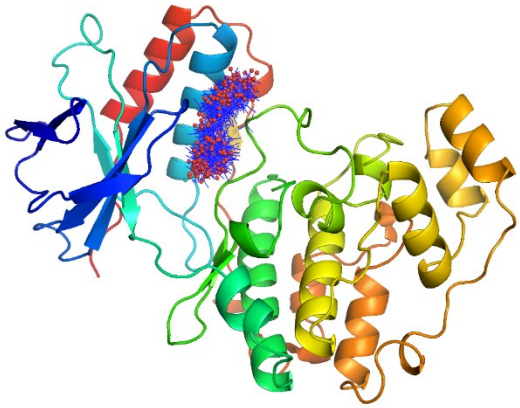

Figure S4. Using The PyMOL Molecular Graphics System (Version 1.8 Schrödinger, LLC) and the plugin MTSSL Wizard rotamers for the spin label were simulated.

Spectral simulations

EPR spectra were analyzed using Matlab R2016a (The MathWorks) using the EasySpin toolbox and the chili function (5.0.16).[3] While varying simulation parameters, the least-square fits were performed. For all simulations, g = [g_x g_y g_z] = [2.00906 2.00687 2.003] were chosen.[4]

Spectral simulations of inhibitor dependent measurements

The spectral simulations are based on a two-component model of two spin ½ systems with a nitrogen nucleus. Both components were simulated using an axial hyperfine tensor, isotropic rotation, an orienting potential [5] and a fixed linewidth using an iterative approach. Using the spectrum of apo p38α with a high content of component S_a and a small portion of component S_B , spectral parameters for S_a including the weighing factor *a* were changed while keeping all parameters for S_B fixed. This optimized system was then used as a fixed component while varying the parameters for B in a spectrum with a high content of the inhibitor-induced conformation. The parameters of the spectral simulation for both components (rotational correlation time, A- and g-tensors and coefficients of the orienting potentials) are given in Table S3.

The spectral fits are deviating from the experimental data beyond the level of noise. Therefore, they contain a significant error. The estimation of this error was done by gradually changing the weighting factors of both components until the deviation of the simulation and experiment was significantly degraded (rmsd increased by 3% from approximately 0.048) . The error estimation was also accounted for in the temperature dependent measurements using error propagation.

Table S2. Parameters used for spectral simulations shown in Figure 2.

	t_{rot} [ns][a]	A_{xx}=A_{yy} [MHz]	A_{zz} [MHz]	linewidth [mT]	g= [g_x g_y g_z]	Orienting potential coefficients $\lambda_{2,0}$, $\lambda_{2,2}$, $\lambda_{4,0}$, $\lambda_{4,2}$, $\lambda_{4,4}$ [kT]
S_A	5.5	13	101.38	0.11	[2.00906 2.00687 2.003]	1.04, 1.46, 0.90, -3.94, -2.43
S_B	0.97	13	111.01	0.11	[2.00906 2.00687 2.003]	0.14, 1.37, -3.96, 0, 0

Spectral simulations of temperature dependent measurements

In order to facilitate data analysis of a large series of experimental data by drastically reducing the computational effort, we decided to use a simplified simulation approach. Allowing for anisotropic rotation and without an orienting potential, describing the experiment with a slightly reduced quality (see Figure S4) is feasible. However, the spectral component weights required for data interpretation obtained by the simplified simulation approach are similar to those obtained by the full model (Table S5). Thus, we chose to use the simplified simulation approach for the spectral analysis of the temperature dependent datasets. In order to account for viscosity changes of the solvent for different temperatures, the effective changes on the spin label's rotational correlation time was estimated according to Cheng (2008).[6] Therefore, a change of $\Delta \log T_{corr} = 0.2$ was allowed during spectral simulations.

Van 't Hoff analysis

Temperature dependent data was collected at temperatures between 5°C and 32.5°C. In this range, no decomposition of the protein-spin label complex was apparent in the EPR spectra. The resulting equilibrium ratios were used to calculate the reaction constant K for the two-state transition and collected in a Van 't Hoff plot of ln(K) over 1/T. The slope of the regression line reflects $-\Delta H/R$ (with R being the gas constant) while the intercept is given by $\Delta S/R$. Using error propagation starting from the initially approximated error for a and a weighted linear fit, the resulting error in ΔH and ΔS was calculated.

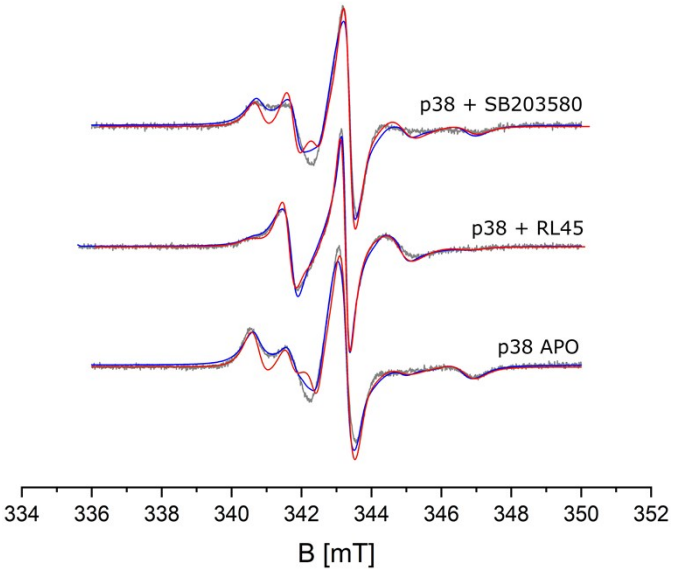

Figure S5. Exemplary comparison of the experimental results (grey) with the spectral simulation with (blue) and without (red) an orienting potential for the apo p38α and after the addition of RL45 / SB203580.

Table S3. Parameters used for temperature series.

	t_{rot} [ns][a]	$A_{xx}=A_{yy}$ [MHz]	A_{zz} [MHz]	linewidth [mT]	g= [g_x g_y g_z]
S_A	see Table S4-S11	13	100.13	0.11	[2.00906 2.00687 2.003]
S_B	see Table S4-S11	15.67	99.56	0.11	[2.00906 2.00687 2.003]

[a] Anisotropic rotational diffusion was assumed for S_B while simulations for S_A are based on isotropic rotational diffusion.

Table S4. Comparison of the spectral simulations with and without the use of an orienting potential and the resulting weighting parameter a.

a for:	p38α apo	+SKF-86002	+skepinone-L	+ SB203580	+RL45	+ RL48	+sorafenib	+ regorafenib
With Orienting Potential	0.89 ± 0.025	0.70 ± 0.05	0.68 ± 0.05	0.76 ± 0.05	0.28 ± 0.05	0.37 ± 0.05	0.47 ± 0.05	0.51 ± 0.05
Without orienting potential	0.88 ± 0.025	0.69 ± 0.05	0.67 ± 0.05	0.69 ± 0.05	0.38 ± 0.05	0.39 ± 0.05	0.48 ± 0.05	0.52 ± 0.05

Results and Discussion

Temperature dependencies

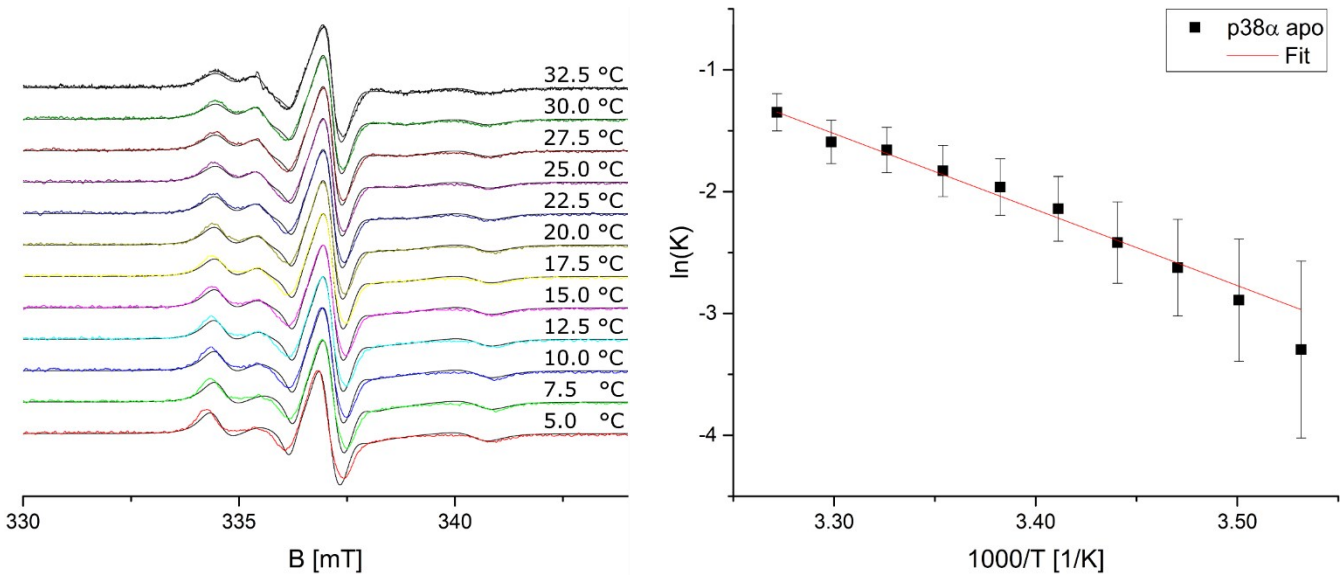

Figure S6. Left: Temperature dependent EPR Spectra of p38α (88 µM) with corresponding spectral simulations (black). Right: Van 't Hoff plots for the reaction constant in dependency of the inverse temperature.

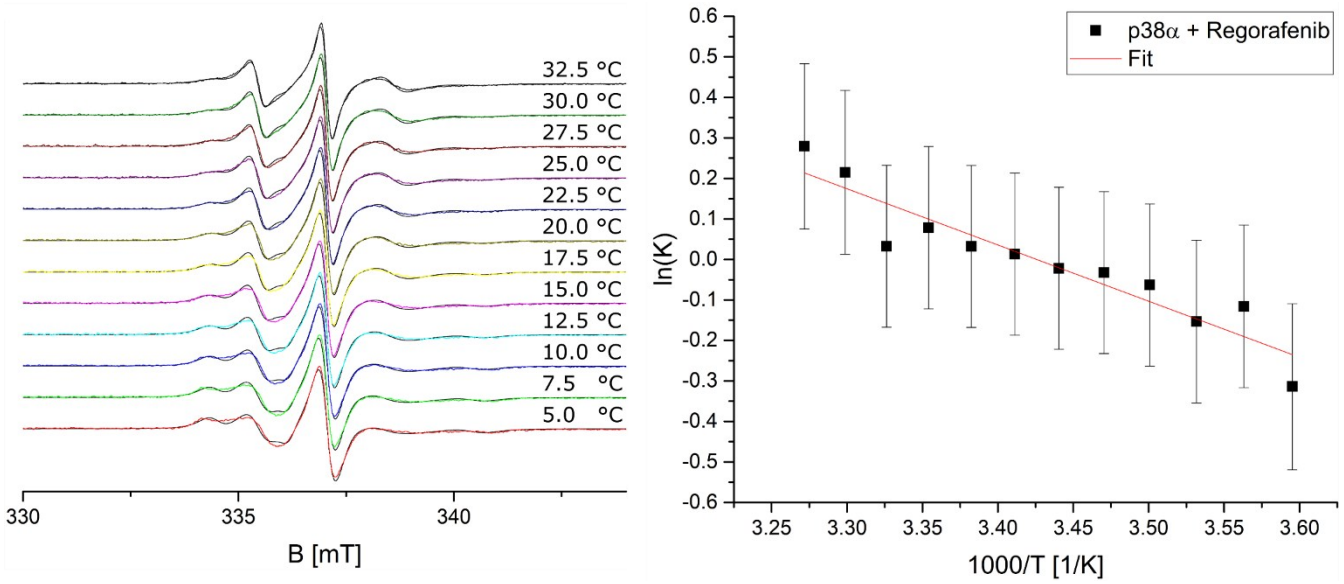

Figure S7. Left: Temperature dependent EPR Spectra of p38α (88 µM) after addition of 6 molar equivalents of Regorafenib with corresponding spectral simulations (black). Right: Van 't Hoff plots for the reaction constant in dependency of the inverse temperature.

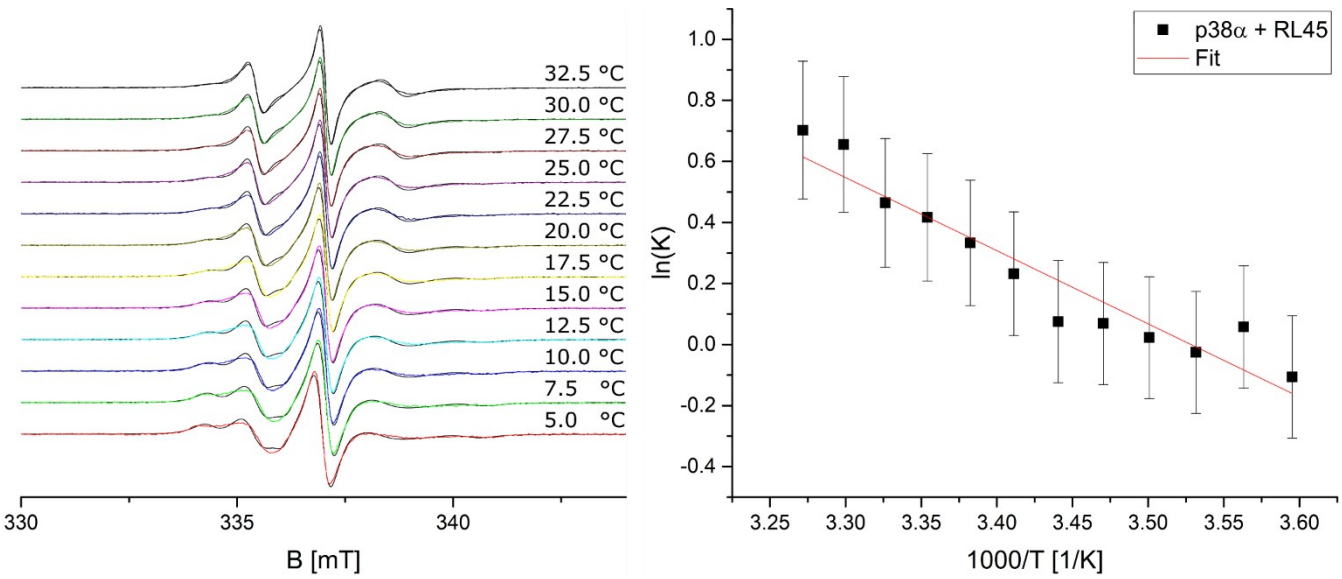

Figure S8. Left: Temperature dependent EPR Spectra of p38α (88 µM) after addition of 6 molar equivalents of RL45 with corresponding spectral simulations (black). Right: Van 't Hoff plots for the reaction constant in dependency of the inverse temperature.

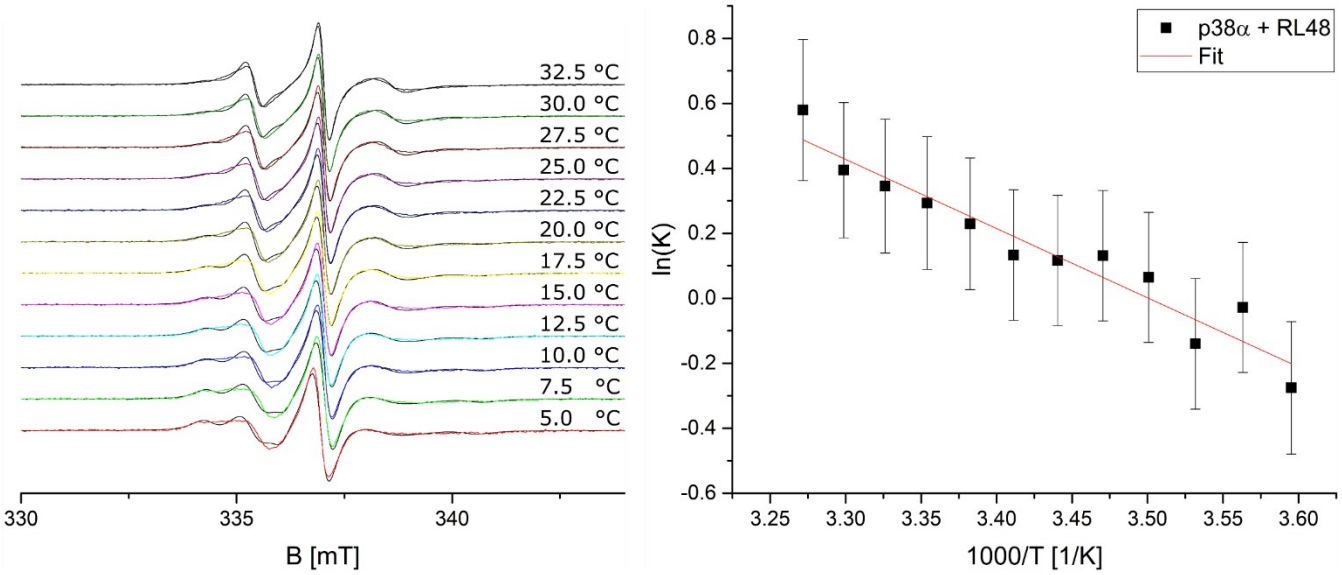

Figure S9. Left: Temperature dependent EPR Spectra of p38α (88 µM) after addition of 6 molar equivalents of RL48 with corresponding spectral simulations (black). Right: Van 't Hoff plots for the reaction constant in dependency of the inverse temperature.

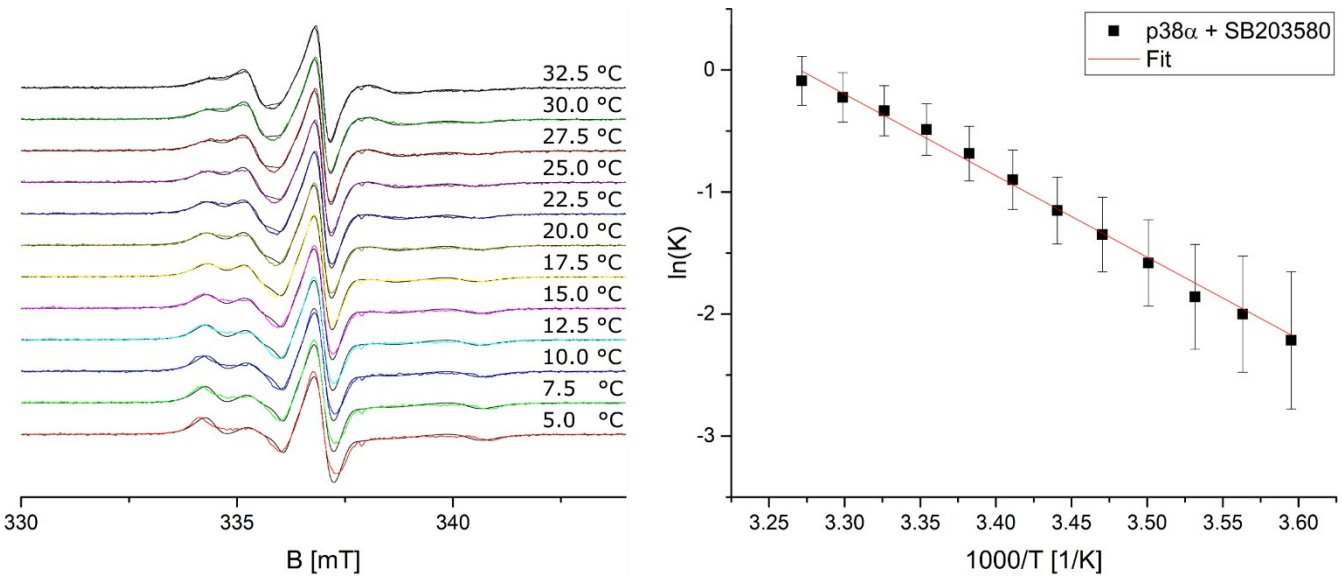

Figure S10. Left: Temperature dependent EPR Spectra of p38α (88 µM) after addition of 6 molar equivalents of SB203580 with corresponding spectral simulations (black). Right: van t'Hoff plots for the reaction constant in dependency of the inverse temperature.

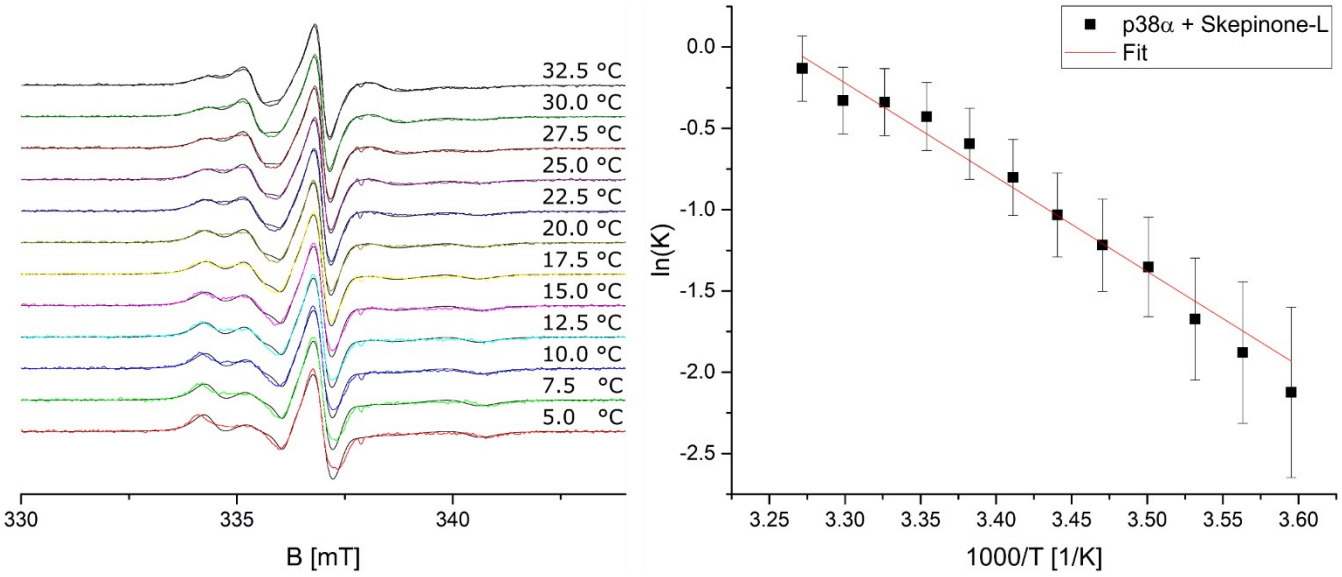

Figure S11 Left: Temperature dependent EPR Spectra of p38α (88 µM) after addition of 6 molar equivalents of Skepinone-L with corresponding spectral simulations (black). Right: Van 't Hoff plots for the reaction constant in dependency of the inverse temperature.

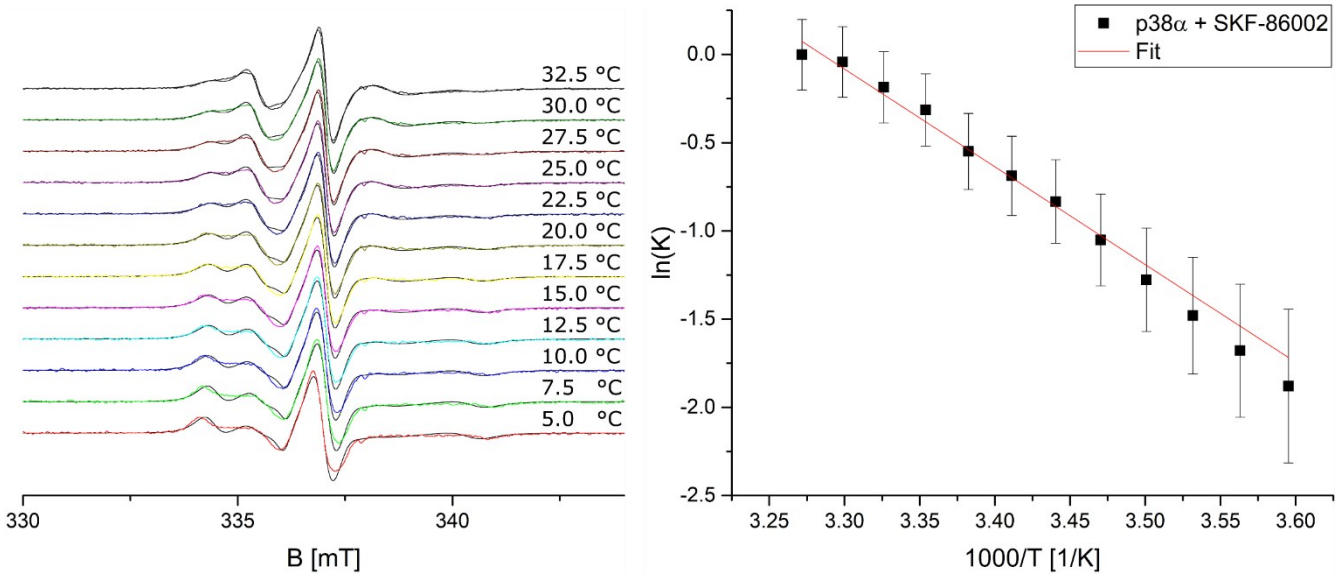

Figure S12. Left: Temperature dependent EPR Spectra of p38α (88 µM) after addition of 6 molar equivalents of SKF-86002 with corresponding spectral simulations (black). Right: Van 't Hoff plots for the reaction constant in dependency of the inverse temperature.

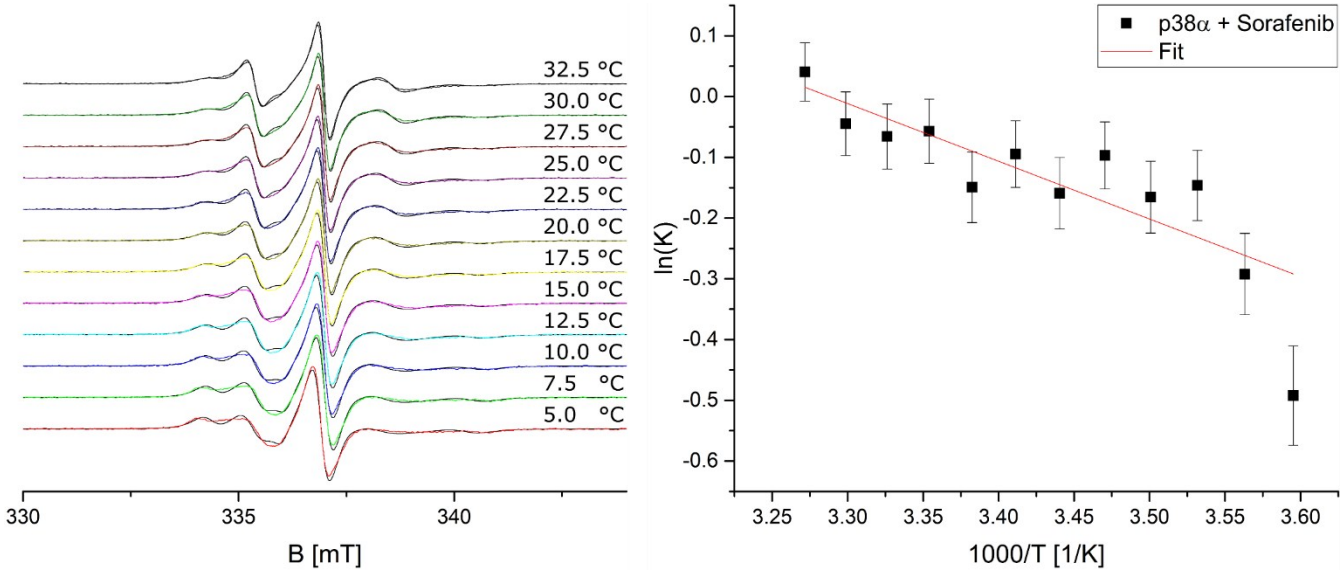

Figure S13. Left: Temperature dependent EPR Spectra of p38α (88 µM) after addition of 6 molar equivalents of Sorafenib with corresponding spectral simulations (black). Right: Van 't Hoff plots for the reaction constant in dependency of the inverse temperature.

Simulation parameters for temperature-dependent measurements

Shown below are the experimental parameters used for the temperature-dependent measurements. All the rotational correlation times have been divided by 1 second and are shown as the negative common logarithm.

Table S5. Rotational correlation times used for simulation of p38α without inhibitor.

Temperature	$-\log(t_{rot})$, S_A	$-\log(t_{rot,1})$, S_B	$-\log(t_{rot,2})$, S_B	$-\log(t_{rot,3})$, S_B
5.0 °C	-7.9540	-7.362	-9.1121	-8.4947
7.5 °C	-7.9964	-7.113	-9.3534	-8.4462
10.0 °C	-7.9967	-7.113	-9.0381	-8.845
12.5 °C	-7.9933	-7.3452	-9.0381	-8.845
15 °C	-8.0082	-7.113	-9.0381	-8.845
17.5 °C	-8.0220	-7.363	-9.0381	-8.845
20.0 °C	-8.0104	-7.113	-9.0381	-8.8316
22.5 °C	-8.0305	-7.4526	-9.0381	-8.8141
25.0 °C	-8.0613	-7.113	-9.0381	-8.845
27.5 °C	-8.0569	-7.2528	-9.0381	-8.845
30.0 °C	-8.0707	-7.5045	-9.0381	-8.845
32.5 °C	-8.0714	-7.113	-9.0381	-8.8033

Table S6. Rotational correlation times used for simulation of p38α after addition of 6 molar equivalents of SB203580.

Temperature	$-\log(t_{rot})$, S_A	$-\log(t_{rot,1})$, S_B	$-\log(t_{rot,2})$, S_B	$-\log(t_{rot,3})$, S_B
5.0 °C	-7.9714	-7.1593	-9.0381	-8.7598
7.5 °C	-7.9796	-7.113	-9.0381	-8.7804
10.0 °C	-8.0197	-7.4597	-9.0381	-8.7221
12.5 °C	-8.0170	-7.113	-9.0381	-8.7662
15 °C	-8.0502	-7.113	-9.0381	-8.7297
17.5 °C	-8.0750	-7.113	-9.0381	-8.7394
20.0 °C	-8.0526	-7.2931	-9.0381	-8.7335
22.5 °C	-8.0601	-7.1293	-9.0386	-8.7308
25.0 °C	-8.0639	-7.113	-9.0381	-8.7402
27.5 °C	-8.0776	-7.1284	-9.0399	-8.7631
30.0 °C	-8.0772	-7.3789	-9.0384	-8.8098
32.5 °C	-8.0823	-7.283	-9.0683	-8.7726

Table S7. Rotational correlation times used for simulation of p38α after addition of 6 molar equivalents of Skepinone-L.

Temperature	$-\log(t_{rot})$, S_A	$-\log(t_{rot,1})$, S_B	$-\log(t_{rot,2})$, S_B	$-\log(t_{rot,3})$, S_B
5.0 °C	-7.9556	-7.113	-9.0383	-8.716
7.5 °C	-7.9860	-7.113	-9.0381	-8.7024
10.0 °C	-8.0042	-7.113	-9.0381	-8.7775
12.5 °C	-7.9981	-7.113	-9.0381	-8.7453
15 °C	-8.0251	-7.492	-9.0381	-8.6938
17.5 °C	-8.0445	-7.1546	-9.0381	-8.7672
20.0 °C	-8.0292	-7.1464	-9.0381	-8.7637
22.5 °C	-8.0367	-7.4262	-9.0381	-8.7125
25.0 °C	-8.0413	-7.2034	-9.0489	-8.7435
27.5 °C	-8.0587	-7.113	-9.0755	-8.7517
30.0 °C	-8.0823	-7.113	-9.1209	-8.7545
32.5 °C	-8.0748	-7.113	-9.0934	-8.7785

Table S8. Rotational correlation times used for simulation of p38α after addition of 6 molar equivalents of SKF-86002.

Temperature	$-\log(t_{rot})$, S_A	$-\log(t_{rot,1})$, S_B	$-\log(t_{rot,2})$, S_B	$-\log(t_{rot,3})$, S_B
5.0 °C	-7.9518	-7.1667	-9.0381	-8.6949
7.5 °C	-7.9571	-7.113	-9.0381	-8.7794
10.0 °C	-7.9920	-7.113	-9.0381	-8.6857
12.5 °C	-8.0197	-7.1135	-9.0381	-8.7362
15 °C	-8.0212	-7.1556	-9.0381	-8.7104
17.5 °C	-8.0178	-7.113	-9.0381	-8.7316
20.0 °C	-8.0393	-7.2531	-9.0381	-8.7211
22.5 °C	-8.0696	-7.4924	-9.0381	-8.7114
25.0 °C	-8.0713	-7.3278	-9.0392	-8.7385
27.5 °C	-8.0596	-7.113	-9.0637	-8.7533
30.0 °C	-8.0639	-7.113	-9.0685	-8.7689
32.5 °C	-8.0823	-7.113	-9.1079	-8.7686

Table S9. Rotational correlation times used for simulation of p38α after addition of 6 molar equivalents of RL45.

Temperature	$-\log(t_{rot})$, S_A	$-\log(t_{rot,1})$, S_B	$-\log(t_{rot,2})$, S_B	$-\log(t_{rot,3})$, S_B
5.0 °C	-7.9671	-7.113	-9.0381	-8.6921
7.5 °C	-7.9541	-7.113	-9.0463	-8.7001
10.0 °C	-8.0161	-7.2917	-9.1017	-8.6954
12.5 °C	-8.0449	-7.3314	-9.1356	-8.6953
15 °C	-8.0479	-7.113	-9.1687	-8.7131
17.5 °C	-8.0816	-7.113	-9.2026	-8.724
20.0 °C	-8.0823	-7.113	-9.2098	-8.7357
22.5 °C	-8.0823	-7.113	-9.2386	-8.7391
25.0 °C	-8.0823	-7.113	-9.2599	-8.7549
27.5 °C	-8.0823	-7.113	-9.2739	-8.7976
30.0 °C	-8.0823	-7.113	-9.2948	-8.7747
32.5 °C	-8.0823	-7.113	-9.3208	-8.7913

Table S10. Rotational correlation times used for simulation of p38α after addition of 6 molar equivalents of RL48.

Temperature	$-\log(t_{rot})$, S_A	$-\log(t_{rot,1})$, S_B	$-\log(t_{rot,2})$, S_B	$-\log(t_{rot,3})$, S_B
5.0 °C	-7.9828	-7.113	-9.056	-8.6689
7.5 °C	-7.9634	-7.113	-9.0383	-8.6824
10.0 °C	-8.0030	-7.113	-9.0874	-8.7154
12.5 °C	-8.0113	-7.113	-9.091	-8.714
15 °C	-8.0083	-7.1863	-9.1071	-8.7103
17.5 °C	-8.0499	-7.113	-9.1544	-8.7272
20.0 °C	-8.0549	-7.113	-9.1849	-8.7418
22.5 °C	-8.0793	-7.113	-9.2099	-8.7387
25.0 °C	-8.0823	-7.3149	-9.2238	-8.7449
27.5 °C	-8.0823	-7.4481	-9.2368	-8.7505
30.0 °C	-8.0823	-7.3819	-9.2642	-8.7328
32.5 °C	-8.0622	-7.3795	-9.2721	-8.7454

Table S11. Rotational correlation times used for simulation of p38α after addition of 6 molar equivalents of Sorafenib.

Temperature	$-\log(t_{rot})$, S_A	$-\log(t_{rot,1})$, S_B	$-\log(t_{rot,2})$, S_B	$-\log(t_{rot,3})$, S_B
5.0 °C	-7.9665	-7.304	-9.0381	-8.6944
7.5 °C	-7.9447	-7.1915	-9.0381	-8.7217
10.0 °C	-7.9434	-7.1477	-9.039	-8.7277
12.5 °C	-7.9743	-7.299	-9.0761	-8.7321
15 °C	-7.9909	-7.113	-9.0992	-8.7337
17.5 °C	-8.0139	-7.113	-9.141	-8.7453
20.0 °C	-8.0233	-7.161	-9.1593	-8.7474
22.5 °C	-8.0497	-7.3626	-9.194	-8.7438
25.0 °C	-8.0656	-7.113	-9.2071	-8.7946
27.5 °C	-8.0823	-7.113	-9.2441	-8.779
30.0 °C	-8.0823	-7.4506	-9.2646	-8.7739
32.5 °C	-8.0823	-7.1144	-9.2858	-8.8078

Table S12. Rotational correlation times used for simulation of p38α after addition of 6 molar equivalents of Regorafenib.

Temperature	$-\log(t_{rot})$, S_A	$-\log(t_{rot,1})$, S_B	$-\log(t_{rot,2})$, S_B	$-\log(t_{rot,3})$, S_B
5.0 °C	-7.9544	-7.304	-9.0381	-8.6806
7.5 °C	-7.9514	-7.113	-9.0381	-8.7059
10.0 °C	-7.9709	-7.113	-9.0696	-8.7213
12.5 °C	-7.9852	-7.2439	-9.0987	-8.7141
15 °C	-7.9976	-7.113	-9.1236	-8.7212
17.5 °C	-8.0411	-7.113	-9.1588	-8.738
20.0 °C	-8.0369	-7.113	-9.1741	-8.7413
22.5 °C	-8.0622	-7.3781	-9.2057	-8.7468
25.0 °C	-8.0823	-7.113	-9.2322	-8.764
27.5 °C	-8.0823	-7.113	-9.2597	-8.7691
30.0 °C	-8.0823	-7.113	-9.2721	-8.7917
32.5 °C	-8.0823	-7.2632	-9.2867	-8.7962

References

[1] J. R. Simard, M. Getlik, C. Grütter, V. Pawar, S. Wulfert, M. Rabiller, D. Rauh, Development of a fluorescent-tagged kinase assay system for the detection and characterization of allosteric kinase inhibitors, *J Am Chem Soc* **2009**, *131*, 13286-13296.

[2] G. Hagelueken, R. Ward, J. H. Naismith, O. Schiemann, MtsslWizard: in silico spin-labeling and generation of distance distributions in PyMOL, *Appl Magn Reson* **2012**, *42*, 377-391.

[3] S. Stoll, A. Schweiger, EasySpin, a comprehensive software package for spectral simulation and analysis in EPR, *J Magn Reson* **2006**, *178*, 42-55.

[4] S. Steigmiller, M. Borsch, P. Graber, M. Huber, Distances between the b-subunits in the tether domain of F0F1-ATP synthase from E. coli, *Bba-Bioenergetics* **2005**, *1708*, 143-153.

[5] K. A. Earle, Budil, David E., in *Advanced ESR Methods in Polymer Research*, **2006**.

[6] N. S. Cheng, Formula for the viscosity of a glycerol-water mixture, *Ind Eng Chem Res* **2008**, *47*, 3285-3288.